AD-A087 027 PENNSYLVANIA STATE UNIV UNIVERSITY PARK APPLIED RESE--ETC F/G 20/4
A SPLINE RELAXATION PROCEDURE FOR CALCULATING AXISYMMETRIC FLOW--ETC(U)
MAY 80 G H HOFFMAN N00024-79-C-6043
UNCLASSIFIED ARL/PSU/TM-80-108 NL

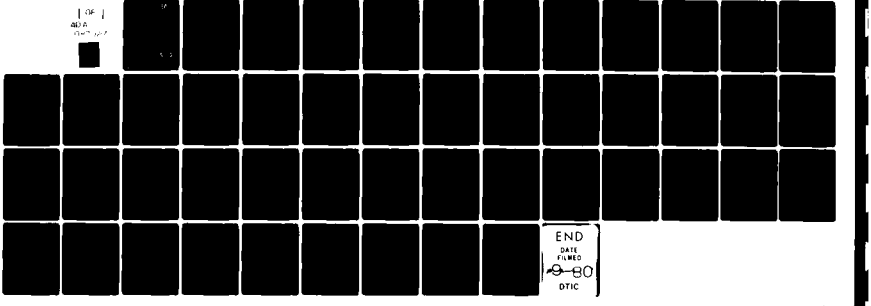

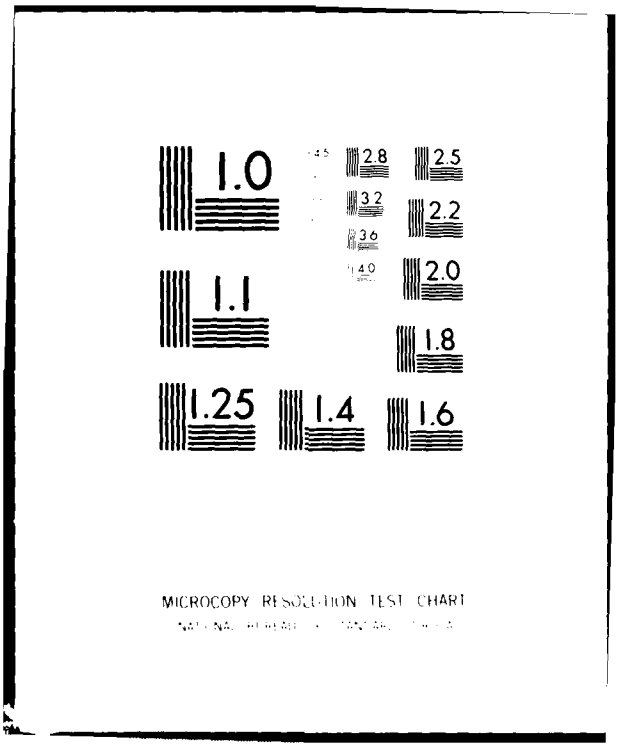
1.0
2.8
2.5
3.2
2.2
3.6
4.0
2.0
1.1
1.8
1.25
1.4
1.6
MICROCOPY RESOLUTION TEST CHART

N.H.

ADA087027

12 B.S. LEVEL II

A SPLINE RELAXATION PROCEDURE FOR CALCULATING AXISYMMETRIC FLOW FIELDS ABOUT BODY/PROPELLER COMBINATIONS; I. FROZEN VORTICITY AND POTENTIAL FLOWS

G. H. Hoffman

Technical Memorandum
File No. TM 80-108
14 May 1980
Contract No. N00024-79-C-6043

Copy No. 36

The Pennsylvania State University
APPLIED RESEARCH LABORATORY
Post Office Box 30
State College, PA 16801

DTIC
ELECTE
JUL 23 1980
S D
B

Approved for Public Release
Distribution Unlimited

NAVY DEPARTMENT

NAVAL SEA SYSTEMS COMMAND

DDC FILE COPY

80 7 21 032

UNCLASSIFIED

SECURITY CLASSIFICATION OF THIS PAGE (When Data Entered)

REPORT DOCUMENTATION PAGE	READ INSTRUCTIONS BEFORE COMPLETING FORM
1. REPORT NUMBER: TM-80-108	2. GOVT ACCESSION NO.: AD-A087027	3. RECIPIENT'S CATALOG NUMBER
4. TITLE (and Subtitle): A SPLINE RELAXATION PROCEDURE FOR CALCULATING AXISYMMETRIC FLOW FIELDS ABOUT BODY/PROPELLER COMBINATIONS, I. FROZEN VORTICITY AND POTENTIAL FLOWS.	5. TYPE OF REPORT & PERIOD COVERED: Technical Memorandum
	6. PERFORMING ORG. REPORT NUMBER
7. AUTHOR(s): G. H. Hoffman	8. CONTRACT OR GRANT NUMBER(s): N00024-79-C-6043
9. PERFORMING ORGANIZATION NAME AND ADDRESS: Applied Research Laboratory, P. O. Box 30, State College, PA 16801	10. PROGRAM ELEMENT, PROJECT, TASK AREA & WORK UNIT NUMBERS
11. CONTROLLING OFFICE NAME AND ADDRESS: Naval Sea Systems Command - Code NSEA 634-31, Department of the Navy, Washington, DC 20362	12. REPORT DATE: 14 May 1980
	13. NUMBER OF PAGES: 43
14. MONITORING AGENCY NAME & ADDRESS (if different from Controlling Office)	15. SECURITY CLASS. (of this report): UNCLASSIFIED
	15a. DECLASSIFICATION/DOWNGRADING SCHEDULE

16. DISTRIBUTION STATEMENT (of this Report)

Approved for Public Release. Distribution Unlimited

~~Per NAVSEA July 3, 1980~~

17. DISTRIBUTION STATEMENT (of the abstract entered in Block 20, if different from Report)

18. SUPPLEMENTARY NOTES

19. KEY WORDS (Continue on reverse side if necessary and identify by block number)

axisymmetric, flow, calculation

20. ABSTRACT (Continue on reverse side if necessary and identify by block number)

A general numerical solution method is presented for calculating incompressible axisymmetric viscous/turbulent flow in the tail-near wake region of a body-propeller combination. The method makes use of the parabolic vorticity transport approximation in conjunction with polynomial splines to achieve sufficient accuracy in high flow gradient regions with as few grid points as possible. A sheared body fitted

(continuing)

DD FORM 1 JAN 73 1473 EDITION OF 1 NOV 65 IS OBSOLETE

UNCLASSIFIED

SECURITY CLASSIFICATION OF THIS PAGE (When Data Entered)

391007

coordinate system is used and the numerical solution of the finite difference equations is obtained by standard line overrelaxation. This report presents the details of the method for the first phase of the work where the vorticity transport equation is omitted (frozen vorticity flow). Sample potential flow and frozen vorticity solutions are presented with no propeller present.

Subject: A Spline Relaxation Procedure for Calculating Axisymmetric Flow Fields about Body/Propeller Combinations; I. Frozen Vorticity and Potential Flows.

References: See page 34.

Abstract: A general numerical solution method is presented for calculating incompressible axisymmetric viscous/turbulent flow in the tail-near wake region of a body-propeller combination. The method makes use of the parabolic vorticity transport approximation in conjunction with polynomial splines to achieve sufficient accuracy in high flow gradient regions with as few grid points as possible. A sheared body fitted coordinate system is used and the numerical solution of the finite difference equations is obtained by standard line overrelaxation. This report presents the details of the method for the first phase of the work where the vorticity transport equation is omitted (frozen vorticity flow). Sample potential flow and frozen vorticity solutions are presented with no propeller present.

Acknowledgment: This work was sponsored by Naval Sea Systems Command, Code NSEA-63R-31.

TABLE OF CONTENTS

LIST OF FIGURES

ACCESSION for
NTIS White Section
DDC Buff Section
UNANNOUNCED
JUSTIFICATION
BY
DISTRIBUTION/AVAILABILITY CODES
Dist. AVAIL. and/or SPECIAL
A

NOMENCLATURE

C_p pressure coefficient

F reduced vorticity - defined by Eq. (5)

G perturbation stream function - defined by Eq. (7)

H total head - defined by Eq. (90)

ℓ spline derivative approximation of $\frac{\partial G}{\partial \eta}$

L spline derivative approximation of $\frac{\partial^2 G}{\partial \eta^2}$

L^* body length (dimensional)

N_η number grid intervals in η-direction

N_ξ number grid intervals in ξ-direction

r radial distance

r_B body radius

r_E outer cylinder radius (where far field boundary condition applied)

u velocity component in x-direction

v velocity component in r-direction

x axial distance

x_0 axial coordinate of initial line in computational domain

x_1 axial coordinate of final line in computational domain

U_∞^* free-stream speed (dimensional)

$\Delta\eta$ step size in η-direction

$\Delta\xi$ step size in ξ-direction

η transformed radial coordinate

ξ transformed axial coordinate

ζ vorticity magnitude

All other quantities are defined in the text.

NOMENCLATURE (cont.)

All quantities in the text are made dimensionless as follows:

distances by L^*

velocities by U_∞^*

stream function by $L^{*2}\ U_\infty^*$

vorticity by U_∞^*/L^*

I. INTRODUCTION

The calculation of the flow field in the vicinity of the tail of a propeller/body combination is complicated by three effects which interact strongly with one another. These effects are:

1. The curving outer streamlines adjusting to the upcoming wake line of symmetry induces a significant pressure gradient in the boundary layer normal to the main flow direction.
2. The outer flow (where vorticity is negligible) is displaced by the rapidly thickening boundary layer near the tail.
3. The streamlines near the tail are modified by the presence of the propeller.

The treatment of normal pressure gradient and displacement effects has usually involved retaining the division of the flow field into a boundary layer and inviscid flow. These effects are then accounted for approximately by the displacement body approach where the boundary-layer displacement thickness is added to the original body [1 - 3],* or by patching the boundary layer to the inviscid outer flow at the edge of the boundary layer [4, 5]. In either case the solution must be found by iteration because of an initially unknown boundary location. The solution process is complicated by the iteration being notoriously sensitive in the tail region where streamline curvature is greatest. Consequently such a procedure requires a great deal of judgment on the part of the user.

The effects of a propeller are often accounted for by a frozen vorticity calculation in conjunction with an actuator disk to represent the propeller. The boundary layer establishes the vorticity distribution

*Numbers in brackets designate References at end of text.

at some station upstream of the propeller. Then the flow is calculated through the actuator disk as though it were inviscid but rotational - hence the name "frozen" vorticity. The result is a modified flow field which approximately accounts for the influence of the propeller. Huang, et al. [2] have combined this type of calculation with the displacement body idea.

The first treatment of all three effects together where simplifying assumptions were held to a minimum was by Schetz and Favin [6, 7]. Their approach is based on the full axisymmetric time-averaged unsteady Navier-Stokes equations with the propeller modeled by an actuator disk or zone and the turbulence field modeled by a simplified turbulent kinetic energy transport equation which depends only on the streamwise distance.

The solution strategy followed by Schetz and Favin was to solve the Navier-Stokes equations only where absolutely necessary, i.e. in a restricted domain, as shown in Fig. 1, whose size is dictated on physical grounds. Referring to Fig. 1, in domain 1 the effects of viscosity are negligible so that the potential flow approximation is valid, in domain 2 the conventional first-order boundary-layer equations hold and in domain 3 the full Navier-Stokes equations must be used. Domain 3 is the region where the three strong interaction effects, mentioned previously, are present.

Because cylindrical coordinates are used, the solutions obtained by Schetz and Favin were limited to bodies with tails which are either infinitely thin or conical. The conical case was accommodated by using a stair-step grid at the body surface which does not lead to effective step size control in the boundary-layer region. The equations of motion

were solved in stream function-vorticity form using a direct solver for the Poisson equation and the ADI technique for the time-dependent vorticity transport equation.

The aim of the present work is also to solve the strong interaction problem associated with a propeller/body combination with as few simplifications as possible but with more generality than the approach of Schetz and Favin. The present method is designed to handle an arbitrary, smooth, pointed tail shape on which is mounted either an open propeller or a pump-jet (ducted propeller).

The solution strategy to be used is very similar to that of Murphy [8] in his development of an efficient Navier-Stokes solver and consists of the following five elements:

1. A truncated computational domain (similar to Schetz and Favin) is used in the tail-near wake region in which the "thin-layer" version of the time-averaged Navier-Stokes equation is solved. The thin-layer approximation involves neglect of viscous/turbulent diffusion terms in the streamwise direction.
2. The steady-state form of the equations of motion are solved which usually involves many fewer iterations than obtaining a steady-state solution from the unsteady equations.
3. The propeller is modeled by an actuator disk or zone.
4. A non-orthogonal coordinate transformation is used so that an arbitrary, smooth, pointed tail body and actuator disk or zone are families of the coordinate system. Thus boundary conditions are easy to apply and effective step size control can be maintained close to the body surface where flow gradients are large.

5. A fourth-order spline or sixth-order Hermite discretization is used in the direction normal to the main flow so that the region of high flow gradients near the body surface can be resolved with relatively few node points. The result is a more computationally efficient method. Murphy used a generalized Galerkin technique with splined Taylor series expansions to achieve fourth-order accuracy in the direction normal to the main flow. The present approach achieves essentially the same result but requires less algebra to arrive at the numerical algorithm.

The work is being performed in two phases. In phase 1, covered in this report, viscosity and the actuator zone are omitted to simplify the algorithm. Otherwise all the elements of the numerical strategy are present. The intent is to gain an understanding of the proposed method by solving a simpler sub-problem whose solution will then be used as a first guess for the full problem. Thus in phase 1, the problem reduces to the solution of Poisson's equation for the stream function with a "frozen" vorticity distribution established on the upstream computational boundary by the boundary-layer solution. In phase 2, all of the elements of the problem will be included. In this phase the turbulence field will be modeled by a simple two-piece algebraic eddy viscosity model corrected for streamline curvature effects.

II. ANALYSIS

The Frozen Vorticity Equation

In cylindrical coordinates (x, r, θ) with velocity components (u, v, 0) where $\partial/\partial\theta \equiv 0$ (axial symmetry), the vorticity vector has a component in the θ-direction only with magnitude ζ given by

$$\zeta = \frac{\partial v}{\partial x} - \frac{\partial u}{\partial r} \quad . \tag{1}$$

For steady incompressible flow the equation of mass conservation reduces to

$$\frac{\partial}{\partial x}(ru) + \frac{\partial}{\partial r}(rv) = 0 \quad . \tag{2}$$

Mass conservation is satisfied identically by the Stokes stream function defined by

$$ru = \frac{\partial \psi}{\partial r} \quad , \quad rv = -\frac{\partial \psi}{\partial x} \quad . \tag{3}$$

With the aid of the Stokes stream function the vorticity, Eq. (1), becomes

$$\frac{\partial^2 \psi}{\partial r^2} - \frac{1}{r}\frac{\partial \psi}{\partial r} + \frac{\partial^2 \psi}{\partial x^2} = -r\zeta \tag{4}$$

For axially symmetric inviscid rotational flow it can be shown that [9]

$$\zeta = r\,F(\psi) \quad , \tag{5}$$

where $F(\psi)$ is called the reduced vorticity and is determined by conditions at the upstream boundary. In terms of $F(\psi)$, Eq. (4) becomes

$$\frac{\partial^2\psi}{\partial r^2} - \frac{1}{r}\frac{\partial\psi}{\partial r} + \frac{\partial^2\psi}{\partial x^2} = - r^2 F(\psi) \quad . \tag{6}$$

In the far field the flow must approach a uniform stream, i.e. $u \to 1$ as $r \to \infty$. Thus the stream function must behave like $r^2/2$ as r goes to infinity. If this unbounded behavior is subtracted from ψ the result is a perturbation stream function $G(x, r)$ defined by

$$G(x, r) = \psi(x, r) - \frac{r^2}{2} \quad , \tag{7}$$

which is well behaved as $r \to \infty$. Since $r^2/2$ is a particular solution of Eq. (4), G satisfies the same differential equation as ψ, viz.:

$$\frac{\partial^2 G}{\partial r^2} - \frac{1}{r}\frac{\partial G}{\partial r} + \frac{\partial^2 G}{\partial x^2} = - r^2 F(\psi) \quad . \tag{8}$$

For the truncated computational domain shown in Fig. 2 the appropriate boundary conditions are:

$$\psi = 0 \text{ on } r = \begin{cases} r_B \quad , & x_0 \leq x \leq 1 \quad , \\ \\ 0 \quad , & x \geq 1 \quad , \end{cases} \tag{9}$$

$$\psi = \psi_0(r) \quad \text{on } x = x_0 \quad , \quad r_B \leq r \leq r_E \quad , \tag{10}$$

$$\psi = \psi_E(x) \quad \text{on } r = r_E \quad , \quad x \geq x_0 \quad , \tag{11}$$

$$\frac{\partial\psi}{\partial x} = 0 \qquad \text{on } x = x_1 \quad , \quad 0 \leq r \leq r_E \quad . \tag{12}$$

The boundary condition on $x = x_1$, the right-hand boundary, is somewhat arbitrary and could just as well be replaced by $\psi_{xx} = 0$.

Body Fitted Coordinates

For ease of application of boundary conditions a coordinate transformation must be found which maps the body surface and propeller shroud into coordinate surfaces in the mapped plane. In addition, for modeling the propeller by an actuator disk or zone, vertical lines should remain unchanged. The following sheared transformation has these desired properties:

$$\xi = x \tag{13a}$$

$$\eta = \phi_1(x) \cdot r - \phi_2(x) \tag{13b}$$

where $\varphi_1(x)$ and $\varphi_2(x)$ are piecewise continuous functions which depend upon the particular geometry. The transformation applies to a shroud with or without thickness whose leading and trailing edges are sharp, i.e., which has an included angle considerably less than 90 degrees. For blunt leading or trailing edges the transformation breaks down.

Figure 3 illustrates a typical application of Eq. (13) to a body-shroud combination. Because of the particular geometry the region must be divided into five parts. As can be seen, the body is mapped onto part of $\eta = 0$ and the shroud becomes a slit on $\eta = \eta_s$. Figure 3 also illustrates that lines of constant ξ and constant η in the physical plane are generally not orthogonal.

Since the derivatives of $\phi_1(x)$ and $\phi_2(x)$ are discontinous at region boundaries, the transformed differential equation will have coefficients which are also discontinuous at region boundaries. Continuity of

the solution $\psi(\xi, \eta)$ and its derivatives will provide the necessary "jump" conditions at the boundary, as will be seen.

In the present "test" problem we restrict the geometry to a body with no shroud so that only two mapped regions are necessary, as illustrated in Fig. 2. The appropriate transformations are:

Region I: $x_0 \leq x \leq 1$ (aft portion of body)

$$\xi = x \quad , \tag{14a}$$

$$\eta = \frac{r - r_B(x)}{r_E - r_B(x)} \quad , \tag{14b}$$

Region II: $x \geq 1$

$$\xi = x \quad , \tag{15a}$$

$$\eta = \frac{r}{r_E} \quad . \tag{15b}$$

In region II we are merely scaling r to be compatible with region I. The transformation in II is therefore orthogonal. In region I we see that $\eta = 0$ on $r = r_B$ while in region II $\eta = 0$ on $r = 0$. In both regions $\eta = 1$ on $r = r_E$.

Transformed Equation of Motion

By applying the chain rule, Eq. (8) in transformed (ξ, η) coordinates can be written in the following general form valid for regions I and II:

$$a\, G_{\eta\eta} + b\, G_{\xi\eta} + G_{\xi\xi} + d\, G_{\eta} + e = 0 \quad , \tag{16}$$

where

$$a = \hat{A}^2 + \hat{B}^2 \quad , \tag{17}$$

$$b = 2\hat{A} \quad , \tag{18}$$

$$d = \hat{B}\left(\hat{B}_\eta - \frac{1}{r}\right) + \hat{A}_\xi + \hat{A}\hat{A}_\eta \quad , \tag{19}$$

$$e = r^2 F(\psi) \quad , \tag{20}$$

and

$$\hat{A} = \left(\frac{\partial \eta}{\partial x}\right)_r \quad , \tag{21}$$

$$\hat{B} = \left(\frac{\partial \eta}{\partial r}\right)_x \quad . \tag{22}$$

From Eqs. (14) and (15) the mapping derivatives are found to be:

Region I:

$$\hat{A} = \frac{r_B'(\xi)}{r_E - r_B(\xi)}\,(\eta - 1) \quad , \tag{23}$$

$$\hat{B} = \frac{1}{r_E - r_B(\xi)} \quad , \tag{24}$$

$$\hat{A}_\xi = \left\{ \frac{r_B''(\xi)}{r_E - r_B(\xi)} + \left[\frac{r_B'(\xi)}{r_E - r_B(\xi)}\right]^2 \right\} (\eta - 1) \quad , \tag{25}$$

$$\hat{A}_\eta = \frac{r_B'(\xi)}{r_E - r_B(\xi)} \quad , \tag{26}$$

$$\hat{B}_\eta = 0 \quad . \tag{27}$$

Region II:

$$\hat{A} = \hat{A}_\xi = \hat{A}_\eta = 0 \quad , \tag{28}$$

$$\hat{B} = \frac{1}{r_E} \quad , \tag{29}$$

$$\hat{B}_\eta = 0 \quad . \tag{30}$$

From Eqs. (9) - (12) together with Eq. (7), the boundary conditions for the transformed equation of motion are:

$$G = -\frac{1}{2} r_B^2(\xi) \quad , \quad \text{on } \eta = 0 \quad , \quad \xi_0 \leq \xi \leq 1 \quad , \tag{31}$$

$$G = 0 \quad , \quad \text{on } \eta = 0 \quad , \quad \xi \geq 1 \quad , \tag{32}$$

$$G = g(\eta) \quad , \quad \text{on } \xi = \xi_0 \quad , \quad 0 \leq \eta \leq 1 \quad , \tag{33}$$

$$G = G_E(\xi) \quad , \quad \text{on } \eta = 1 \quad , \quad x \geq \xi_0 \quad , \tag{34}$$

$$\frac{\partial G}{\partial \xi} = 0 \quad , \quad \text{on } \xi = \xi_1 \quad , \quad 0 \leq \eta \leq 1 \quad . \tag{35}$$

The boundary conditions must be supplemented by "jump" conditions on the derivatives of G in the transformed plane at $\xi = 1$ so that the solution can be continued from one region to the next. We know that G and its x and r derivatives must be continuous at $\xi = 1$ because the stream function and velocity components are continuous. Thus at $\xi = 1$ we have

$$(G)_- = (\tilde{G})_+ \quad , \qquad (36)$$

$$(G_x)_- = (G_x)_+ \quad , \qquad (37)$$

$$(G_r)_- = (G_r)_+ \quad , \qquad (38)$$

at $x = 1$

where "-" denotes the left-hand limit (in region I), "+" denotes the right-hand limit (in region II) and the tilde denotes the function in region II. The chain rule relating first derivatives in (ξ, η) variables to those in (x, r) variables can be expressed as

$$\left(\frac{\partial}{\partial x}\right)_r = \left(\frac{\partial}{\partial \xi}\right)_\eta + \hat{A}(\xi,\eta)\left(\frac{\partial}{\partial \eta}\right)_\xi \quad , \qquad (39)$$

$$\left(\frac{\partial}{\partial r}\right)_x = \hat{B}(\xi,\eta)\left(\frac{\partial}{\partial \eta}\right)_\xi \quad . \qquad (40)$$

Then with the aid of the chain rule relations, Eqs. (39) - (40), and the mapping derivatives, Eqs. (23) - (24) and (28) - (29), and noting that $B_I(1,\eta) = B_{II}(1,\eta)$ since $r_B(1) = 0$, the jump conditions can be written as

$$(\tilde{G}_\xi)_+ = (G_\xi)_- + \hat{A}_I(1, \eta)(G_\eta)_- \quad , \qquad (41)$$

$$(\tilde{G}_\eta)_+ = (G_\eta)_- \quad . \qquad (42)$$

From Eq. (42) and the fact that $B_\eta = 0$ in regions I and II we also have that

$$(G_{\eta\eta})_+ = (G_{\eta\eta})_- \quad . \qquad (43)$$

We can infer in this case that all the η-derivatives are continuous at $\xi = 1$. Thus the only "jump" occurs in the ξ-derivative, as given by Eq. (41).

Numerical Algorithm

For the frozen vorticity equation the numerical algorithm has been chosen to be almost the same as the one to be used later on for the full problem with viscous/turbulent effects. The reason for this choice was to gain familiarity with the algorithm on a simpler problem.

A combination finite difference and spline representation is used for reasons of accuracy and maintenance of a block tridiagonal matrix structure of the resulting equations. In the streamwise direction, where flow quantities are expected to vary somewhat slowly, centered difference formulas with constant $\Delta\xi$ are used. In the direction normal to the ξ-axis, where flow quantities are expected to vary rapidly near the body (in the viscous/turbulent case), polynomial spline formulas are used to obtain higher-order accuracy.

We now define the following spline derivatives in the η-direction:

$$\left.\begin{aligned} \ell &= G_\eta \quad , \\ L &= G_{\eta\eta} \quad . \end{aligned}\right\} \tag{44}$$

Then the frozen vorticity equation can be written at node point (i, j) as

$$(a\,L + b\,\ell_\xi + G_{\xi\xi} + d\,\ell + e)_{i,\,j} = 0 \quad , \tag{46}$$

where i and j denote the ξ and η coordinate lines respectively. The centered difference approximations in the ξ-direction are:

$$(\ell_\xi)_{i,\,j} = \frac{\ell_{i+1,\,j} - \ell_{i-1,\,j}}{2\Delta\xi} + O(\Delta\xi^2) \quad , \tag{47}$$

$$(G_{\xi\xi})_{i,\,j} = \frac{G_{i-1,\,j} - 2\,G_{i,\,j} + G_{i+1,\,j}}{\Delta\xi^2} + O(\Delta\xi^2) \quad . \tag{48}$$

Upon substitution of the central difference (CD) approximations in Eq. (46) an algebraic expression results for G, ℓ, and L at the nodal points (i-1, j), (i, j), and i+1, j). For the method of solution chosen, spline line overrelaxation (SPLOR), experience has shown that sweeping in the ξ-direction is much more straightforward than in the η-direction because of the piecewise continuous mapping.

For a ξ-sweep using SPLOR the unknowns lie along line i with those on line (i-1) and (i+1) considered known. Thus from Eq. (46), together with the CD approximations, the unknowns at line i are found to be:

$$-\frac{2}{\Delta\xi^2}\,G_{i,\,j} + d_{i,\,j}\,\ell_{i,\,j} + a_{i,\,j}\,L_{i,\,j} = P_{i,\,j} \quad , \tag{49}$$

where,

$$P_{i,\,j} = \frac{b_{i,\,j}}{2\Delta\xi}\,(\ell_{i-1,\,j} - \ell_{i+1,\,j}) - \frac{1}{\Delta\xi^2}\,(G_{i-1,\,j} + G_{i+1,\,j}) - e_{i,\,j} \quad . \tag{50}$$

Because splines are being used in the η-direction Eq. (49) involves unknowns only at j. Equation (49) is valid in both regions I and II except at $\eta = 0$ where the coefficient d becomes unbounded. At $\eta = 0$ a limiting form of Eq. (49) must be found. In addition, a special form of Eq. (49) must be derived for the junction line between regions I and II.

The Junction Line

The junction line is treated by a generalized version of the method originally developed by Chmielewski and Hoffman [10] for SLOR solution of elliptic partial differential equations with discontinuous coefficients. In this method the solution in each region is extended by analytic continuation one step beyond the boundary into the other region. As a result, two lines of "fictitious" unknowns are formed, one on either side of the junction. In the present case the fictitious unknowns can be eliminated beforehand by use of the jump conditions and by approximating ℓ_ξ in region I by a second-order backward difference formula. As a result, a single algebraic equation is obtained on the junction line so that SPLOR can still be used. In the Chmielewski-Hoffman method the system of unknowns on the junction line and two adjacent fictitious lines was not reduced to a single tri-diagonal equation. Consequently point relaxation was used to solve this system, but everywhere else SLOR was used. We note that by proper matrix partitioning the C-H method becomes block tridiagonal so that SPLOR can be used at the junction line.

On the junction line between regions I and II, denoted by i = IJ, ℓ_ξ in region I is approximated by a second-order backward difference formula, viz.:

$$(\ell_\xi)_{IJ,\,j} = \frac{\ell_{IJ-2,\,j} - 4\,\ell_{IJ-1,\,j} + 3\,\ell_{IJ,\,j}}{2\Delta\xi} + O(\Delta\xi^2) \quad . \tag{51}$$

A centered difference formula at i = IJ is still used for $G_{\xi\xi}$. Thus in region I the transformed equation of motion, Eq. (46), becomes at (IJ, j):

$$a_{IJ,\,j}\,L_{IJ,\,j} + b_{IJ,\,j}\left(\frac{\ell_{IJ-2,\,j} - 4\,\ell_{IJ-1,\,j} + 3\,\ell_{IJ,\,j}}{2\Delta\xi}\right)$$

$$+ \frac{G_{IJ-1} - 2\,G_{IJ,\,j} + G^{*}_{IJ+1,\,j}}{\Delta\xi^{2}} + d_{IJ,\,j}\,\ell_{IJ,\,j} + e_{IJ,\,j} = 0 \quad ,$$

where the asterisk denotes a fictitious unknown from the analytic continuation. Solving for unknowns on i = IJ and IJ + 1, we get

$$-\frac{2}{\Delta\xi^{2}}\,G_{IJ,\,j} + \frac{1}{\Delta\xi^{2}}\,G^{*}_{IJ+1,\,j} + \left(d_{IJ,\,j} + \frac{3\,b_{IJ,\,j}}{2\Delta\xi}\right)\ell_{IJ,\,j}$$

$$+ a_{IJ,\,j}\,L_{IJ,\,j} = Q_{j} \quad , \tag{52}$$

where Q_j consists of quantities considered known and is given by

$$Q_{j} = -\,e_{IJ,\,j} - \frac{1}{\Delta\xi^{2}}\,G_{IJ-1,\,j} - \frac{b_{IJ,\,j}}{2\Delta\xi}\,(\ell_{IJ-2,\,j} - 4\,\ell_{IJ-1,\,j}) \quad . \tag{53}$$

Similarly, in region II Eq. (46) yields the following relation for unknowns on i = IJ and the fictitious unknowns on the line i = IJ - 1:

$$-\frac{2}{\Delta\xi^{2}}\,\tilde{G}_{IJ,\,j} + \frac{1}{\Delta\xi^{2}}\,\tilde{G}^{*}_{IJ-1,\,j} + \tilde{d}_{IJ,\,j}\,\tilde{\ell}_{IJ,\,j} + \tilde{a}_{IJ,\,j}\,\tilde{L}_{IJ,\,j} = \tilde{Q}_{j} \quad , \tag{54}$$

where

$$\tilde{Q}_{j} = -\,e_{IJ,\,j} - \frac{1}{\Delta\xi^{2}}\,\tilde{G}_{IJ+1,\,j} \quad . \tag{55}$$

In obtaining Eq. (54) we have made use of the fact that $b \equiv 0$ in region II.

To obtain a single equation at (IJ, j) we make use of the continuity and jump conditions at i = IJ to eliminate unknowns which arise from the analytic continuation. The continuity conditions were found to be

$$\tilde{G}_{IJ,\,j} = G_{IJ,\,j} \quad ,$$

$$\tilde{\ell}_{IJ,\,j} = \ell_{IJ,\,j} \quad ,$$

$$\tilde{L}_{IJ,\,j} = L_{IJ,\,j} \quad ,$$

and the jump condition was

$$(\tilde{G}_\xi)_{IJ,\,j} = (G_\xi)_{IJ,\,j} + \hat{A}_{IJ,\,j}\, \ell_{IJ,\,j} \quad .$$

Upon replacement of the ξ-derivatives by centered differences, the jump condition becomes

$$\frac{\tilde{G}_{IJ+1,\,j} - \tilde{G}^*_{IJ-1,\,j}}{2\Delta\xi} = \frac{G^*_{IJ+1,\,j} - G_{IJ-1,\,j}}{2\Delta\xi} + \hat{A}_{IJ,\,j}\, \ell_{IJ,\,j} \quad . \tag{56}$$

By combining the continuity conditions and jump condition, as given by Eq. (56), with Eqs. (52) and (54) we can eliminate the unknowns $\tilde{G}^*_{IJ-1,\,j}$ and $G^*_{IJ+1,\,j}$ and arrive at the following equation involving only unknowns on i = IJ:

$$-\frac{2}{\Delta\xi^2} G_{IJ,\,j} + \hat{d}_j\, \ell_{IJ,\,j} + \hat{a}_j\, L_{IJ,\,j} = \hat{P}_j \quad , \tag{57}$$

where: $$\hat{a}_j = \frac{1}{2}\,(a_{IJ,\,j} + \tilde{a}_{IJ,\,j}) \quad , \tag{58}$$

$$\hat{d}_j = \frac{1}{2}\,(d_{IJ,\,j} + \tilde{d}_{IJ,\,j}) + \frac{b_{IJ,\,j}}{4\Delta\xi} \quad , \tag{59}$$

$$\hat{P}_j = -\,e_{IJ,\,j} - \frac{1}{\Delta\xi^2}\,(G_{IJ-1,\,j} + \tilde{G}_{IJ+1,\,j}) - \frac{b_{IJ,\,J}}{4\Delta\xi}\,(\ell_{IJ-2,\,j} - 4\,\ell_{IJ-1,\,j}) \quad . \tag{60}$$

Equation (57) is seen to be of the same form as Eq. (49) for the general case with a modification of the coefficients due to the discontinuity in the mapping derivatives.

Spline Formulas

With the introduction of the spline derivatives ℓ and L we have seen that the frozen vorticity equation yields a single equation for the unknowns G, ℓ, and L at a node point (i, j). To complete the set of equations at (i, j) two polynomial spline formulas relating the function and its η-derivatives must be introduced. For the sake of simplicity we will use spline relations of fourth-order accuracy with variable $\Delta\eta$ as given by Rubin and Khosla [11]. As a further simplification we will use the same spline formula twice, namely $S^1(4, 0)$ (in the nomenclature of Rubin and Khosla) to relate ℓ to G and L to ℓ, viz.:

$$\beta_j G_{i,\,j-1} + \alpha_j G_{i,\,j} + \gamma_j G_{i,\,j+1}$$

$$+ \sigma^2 \ell_{i,\,j-1} + (1 + \sigma)^2 \ell_{i,\,j} + \ell_{i,\,j+1} = 0 \quad , \qquad (61)$$

and

$$\beta_j \ell_{i,\,j-1} + \alpha_j \ell_{i,\,j} + \gamma_j \ell_{i,\,j+1}$$

$$+ \sigma^2 L_{i,\,j-1} + (1 + \sigma)^2 L_{i,\,j} + L_{i,\,j+1} = 0 \quad , \qquad (62)$$

where α, β, γ, and σ are functions only of the step size and are given by

$$\alpha_j = \frac{2(1 - \sigma)(1 + \sigma)^2}{\Delta\eta_{j-1}\,\sigma} \quad , \tag{63}$$

$$\beta_j = \frac{2\sigma^2(2 + \sigma)}{\Delta\eta_{j-1}\,(1 + \sigma)} \quad , \tag{64}$$

$$\gamma_j = -\frac{2(1 + 2\sigma)}{\Delta\eta_{i-1}(1 + \sigma)\sigma} \quad , \tag{65}$$

and

$$\sigma = \sigma_j = \frac{\Delta\eta_j}{\Delta\eta_{j-1}} \quad , \tag{66}$$

$$\Delta\eta_j = \eta_{j+1} - \eta_j \quad . \tag{67}$$

Other polynomial spline approximations can be used in place of Eqs. (61) and (62) depending upon the accuracy desired.

In the (i, j) grid point counting scheme adopted here, i = 1 denotes $\xi = \xi_0$ and i = M + 1 denotes $\xi = \xi_1$ while j = 1 denotes $\eta = 0$ and j = N + 1 denotes $\eta = 1$. Thus the number of grid cells is M by N.

Conditions on Lower and Upper Boundaries

At each boundary ($\eta = 0$ and 1) three equations are needed to determine the unknowns G, ℓ, and L. The first equation is derived from the boundary condition, the second equation from the equation of motion and the third equation from an appropriate spline relation.

On $\eta = 0$ the boundary condition can be expressed as

$$G_{i,\,1} = f(\xi_i) \quad , \tag{68}$$

where,

$$f(\xi_i) = \begin{cases} -\frac{1}{2}\, r_B^{\,2}(\xi_i) \quad , & \xi < 1 \quad , \\ \\ 0 \quad , & \xi \geq 1 \quad . \end{cases} \tag{69}$$

In region I the second relation on $\eta = 0$ is provided by Eq. (49) evaluated at $j = 1$, viz.

$$- \frac{2}{\Delta\xi^2} G_{i,\,1} + d_{i,\,1}\, \ell_{i,\,1} + a_{i,\,1}\, L_{i,\,1} = P_{i,\,1} \,, \quad \xi_0 \leq \xi < 1 \quad . \tag{70}$$

In region II, as well as on the junction line, Eq. (70) is not valid because $d_{i,\,1}$ is unbounded, as already mentioned. We must therefore replace Eq. (70) by an appropriate limit derived from the equation of motion. On $\eta = 0$ the governing differential equation reduces to

$$\frac{1}{r_E^2} \left[L - \lim_{\eta \to 0} \left(\frac{\ell}{\eta} \right) \right] = 0 \quad ,$$

which can only be satisfied if $\ell = 0$. Thus the condition

$$\ell_{i,\,1} = 0 \quad , \quad \xi \geq 1 \quad , \tag{71}$$

replaces Eq. (70) in region II. The final equation is supplied by the spline interpolation polynomial $S^1(4, 0)$, as discussed by Rubin and Khosla [11]. The formula is

$$- \frac{6}{\Delta\eta_1^2} G_{,} \quad + \frac{6}{\Delta\eta_1^2} G_{i,\,2} - \frac{4}{\Delta\eta_1} \ell_{i,\,1} - \frac{2}{\Delta\eta_1} \ell_{i,\,2} - L_{i,\,1} = O(\Delta\eta_1^4) \quad . \tag{72}$$

The use of Eq. (72) means that G is determined to fourth-order accuracy, ℓ to third-order accuracy and L to second-order accuracy.

At the outer boundary, $\eta = 1$, we have the boundary condition common to both regions I and II:

$$G_{i,\,N+1} = G_{E_i} \quad . \tag{73}$$

The second equation is the equation of motion evaluated at $\eta = 1$, viz.:

$$-\frac{2}{\Delta\xi^2} G_{i,\,N+1} + d_{i,\,N+1}\,\ell_{i,\,N+1} + a_{i,\,N+1}\,L_{i,\,N+1} = P_{i,\,N+1} \quad , \tag{74}$$

and the third equation is a spline relation derived from $S^1(4,\,0)$, similar to Eq. (72):

$$-\frac{6}{\Delta\eta_N^2} G_{i,\,N} - \frac{2}{\Delta\eta_N}\,\ell_{i,\,N} + \frac{6}{\Delta\eta_N^2} G_{i,\,N+1} - \frac{4}{\Delta\eta_N}\,\ell_{i,\,N+1} + L_{i,\,N+1} = 0 \quad . \tag{75}$$

Matrix Equations

A compact form of the spline-finite difference equations is obtained by introducing the following three-component column vector of unknowns:

$$Z_{i,\,j} = \begin{bmatrix} G \\ \ell \\ L \end{bmatrix}_{i,\,j} \quad . \tag{76}$$

In terms of $Z_{i,\,j}$ the equations in the field and on the boundaries associated with line i can be written as a block tridiagonal system, viz.:

$$\left.\begin{aligned} &A_1\,Z_1 + C_1\,Z_2 = R_1 \quad , \\ &B_j\,Z_{j-1} + A_j\,Z_j + C_j\,Z_{j+1} = R_j \quad , \quad 2 \le j \le N \quad , \\ &B_{N+1}\,Z_N + A_{N+1}\,Z_{N+1} = R_{N+1} \quad , \end{aligned}\right\} \tag{77}$$

where the i index is understood. In Eq. (77) the coefficients A, B, C are 3 x 3 matrices which depend only on body geometry and step size, and R_j is a three-component column vector of known quantities which is

obtained from the various field and boundary equations. The linear system, Eqs. (77), can be solved by standard lower-upper (L-U) factorization methods - see Keller [12].

Initial and Final Lines

To start the calculation, data on the initial line, i = 1, are required, namely: G, ℓ, and L at each node point. In addition, the reduced vorticity ζ and total head H are needed. With ψ and u as input on the initial line, then G and ℓ are computed from:

$$G = \psi - \frac{r^2}{2} \quad , \tag{78}$$

and

$$\ell = r(r_E - r_B)(u - 1) \quad , \tag{79}$$

where Eq. (79) is derived from the Stokes stream function relation $\psi_r = ru$. The second spline derivative L on the initial line is computed by applying $S^1(4, 0)$ to ℓ. Finally, the reduced vorticity F is determined from Eq. (5) and is stored in a table versus ψ as is the total head H.

At the final line of the computational domain, i = M + 1, the boundary condition is $\psi_\xi = 0$. Using a CD approximation this condition becomes

$$\psi_{M+2,\ j} = \psi_{M,\ j} \quad , \tag{80}$$

and hence $\tilde{P}_{M+1,\ j}$ becomes (note that in region II, b $\equiv$ 0):

$$\tilde{P}_{M+1,\ j} = -\frac{2}{\Delta\xi^2}\tilde{G}_{M,\ j} - \tilde{e}_{M+1,\ j} \quad . \tag{81}$$

Other than this modification the calculation at i = M + 1 is the same as at any other line.

III. RESULTS

Potential Flow Solutions

As a means of testing the present method, potential flow solutions were generated and compared with results obtained from the second-order surface singularity method of Fernandez [13]. Two body shapes were run: the modified spheroid of Patel [14] and the F-57 low-drag body of Parsons and Goodson [15].

The SPLOR solutions for the two test cases were obtained with grid parameters as given in Table 1.

	Modified Spheroid	F-57 Body
x_0	0.4816	0.2280
x_1	2.0368	1.7720
r_E	3.4215	3.2430
N_η	20	20
N_ξ	60	40
$\Delta\eta_1$	0.0054	0.0057
c_η	1.2	1.2

Table 1. Potential Flow SPLOR Grid Parameters.

To simplify the input $G_E(\xi)$ was set to a constant value and r_E taken large enough so that this approximation had negligible effect on the solution. A highly nonuniform step size in η was used to test this feature of the algorithm. As shown in Table 1, the initial $\Delta\eta$ (adjacent to the body) was very small with the ratio of successive steps in η held fixed, i.e.,

$$\frac{\Delta\eta_j}{\Delta\eta_{j-1}} = c_\eta = \text{constant}$$

An overrelaxation factor, r_f, of 1.6 was used throughout the calculations on G, ℓ, and L with no attempt made to determine the optimum r_f. Runs were also made with smaller step sizes than those shown in Table 1 but the change on the numerical solution was negligible.

The numerical solution was considered converged when the largest residual change in G, i.e. $|\delta G^{(N)}| = |G^{(N+1)} - G^{(N)}|$, was less than a prescribed amount, usually 5×10^{-6}. In determining convergence the largest residual change in ℓ or L could just as well have been monitored. As would be expected, for the same number of steps in η those runs with a highly nonuniform distribution took more iterations than those with a uniform distribution to arrive at the same cutoff tolerance. Typical number of iterations to reach a tolerance on δG of 5×10^{-6} was from 40-50 for the parameters given in Table 1 with CPU time on an IBM 370/3033 of about 90 seconds (using double precision arithmetic).

Figures 4 and 5 show the body pressure distribution ($x \leq 1$) as well as the centerline pressure distribution downstream of the body ($x > 1$) for the modified spheroid and F-57 respectively. The surface singularity solution was obtained only on the body. Comparison of SPLOR with surface singularity results shows excellent agreement except very close to the tail. The SPLOR value of C_p at the tail point is seen to be too low. Better agreement with the surface singularity results by SPLOR would probably be obtained by a nonuniform grid in ξ which is denser near the tail point but this is not allowed in the present formulation.

Frozen Vorticity Test Case

The F-57 low-drag body was used as a test case for a frozen vorticity calculation. The initial profile was chosen at $x_0 = 0.7684$ which is at the approximate beginning of the strong interaction region.

The thickness of the vortical layer was taken to be $\eta_\delta \simeq 0.12$ which corresponds approximately to the thickness of the turbulent boundary layer at the initial station for a Reynolds number based on body length of 10^6.

The computed turbulent boundary-layer profile at $x_0 = 0.7684$ was not used for the initial frozen vorticity profile because the values of vorticity near the wall were considered to be too large and the no-slip condition at the wall is inappropriate. Instead, a "manufactured" velocity profile was generated which resembled the turbulent boundary-layer profile but had lower values of vorticity near the wall and a wall slip velocity.

Some care had to be exercised in order to make the manufactured velocity profile compatible with the potential flow at the edge of the vortical layer ($\eta = \eta_\delta$). The procedure finally found to be satisfactory is as follows:

1. We assume that ℓ varies parabolically with η:

$$\ell = a_1 + a_2\eta + a_3\eta^2 \quad , \tag{82}$$

where u is related to ℓ by

$$u = 1 + \frac{\ell}{r(r_E - r_B)} \quad , \tag{83}$$

and the coefficients a_1, a_2, and a_3 are determined from the following conditions:

$\ell(0) = \ell_0$, given wall slip velocity.

$\ell(\eta_\delta) = \ell_1$, u must match with the potential flow value at $\eta = \eta_\delta$.

$\ell'(\eta_\delta) = L_1$, the slopes of the vortical and potential flow profiles must be the same at $\eta = \eta_\delta$.

The resulting initial profile for u is shown in Fig. 6.

2. In the vortical layer G is then obtained by integration of ℓ, which gives

$$G = -\frac{1}{2} r_B^2 + a_1\eta + \frac{1}{2} a_2\eta^2 + \frac{1}{3} a_3\eta^3 \quad . \tag{84}$$

3. The potential flow must be adjusted for $\eta > \eta_\delta$ to account for the vortical layer displacement effect. This correction, which must be applied at each nodal point in the potential flow portion of the profile, is

$$G_{corrected} = G_{potential} + \Delta G_\delta \tag{85}$$

where

$$\Delta G_\delta = (G_{vortical} - G_{potential})_{\eta = \eta_\delta} \tag{86}$$

4. We then obtain the vorticity distribution by making the boundary-layer assumption,

$$\tilde{\zeta} = -\frac{\partial u}{\partial y} \quad .$$

Making use of Eqs. (14b) and (83) the vorticity $\tilde{\zeta}$ is found to be related to ℓ and L by

$$\tilde{\zeta} = - \frac{1}{r(r_E - r_B)} \left(\frac{L}{r_E - r_B} - \frac{\ell}{r} \right) \quad , \tag{87}$$

where L is obtained by differentiation of Eq. (82), viz.:

$$L = \frac{\partial \ell}{\partial \eta} = a_2 + 2a_3 \eta \quad . \tag{88}$$

The vorticity $\tilde{\zeta}$ is generally not zero at the edge of the vortical layer because of the neglect of $\partial v/\partial x$ in the definition. To adjust the vorticity to zero at $\eta = \eta_\delta$ a linear correction with η is applied. The corrected vorticity ζ is therefore:

$$\zeta = \tilde{\zeta} - \tilde{\zeta}(\eta_\delta) \cdot \frac{\eta}{\eta_\delta} \quad . \tag{89}$$

5. The total head distribution in the vortical layer is determined from the dimensionless Bernoulli equation:

$$H = C_p + u^2 + v^2 \quad . \tag{90}$$

In the vortical layer $H < 1$ whereas in the potential flow $H = 1$. In the vortical layer u is known from Eq. (83) but C_p and v are known only at the wall and at $\eta = \eta_\delta$. To obtain C_p and v within the vortical layer we assume that each varies linearly with η which then allows the initial values of H to be computed.

A highly nonuniform grid spacing in η was used with $N_\eta = 26$ and $\Delta\eta_1 = 1.5 \times 10^{-4}$. This distribution gave nine points in the vortical layer.

A comparison of the potential and frozen vorticity pressure distribution on the body and wake centerline as obtained by the SPLOR method is shown in Fig. 7. Also shown are the experimental data of Patel and Lee [16] at a Reynolds number of 1.2×10^6. The frozen vorticity solution generally follows the experimental trend as the tail is approached and has a maximum C_p lower than that of the potential flow solution. Downstream of the tail the frozen vorticity C_p decays too slowly due to the presence of a frozen vorticity "pressure wake" illustrated by the pressure profile plot at $x_0 = 1.309$ in Fig. 8. The pressure wake arises as a result of the total head defect on the initial calculation surface together with the requirement that H remain constant on streamsurfaces.

We empnasize that the point of the present test case is to demonstrate that this portion of the algorithm is working properly. Consequently no attempt has been made to explore the characteristics of boat tail frozen vorticity solutions.

IV. CONCLUSIONS

The present application of spline line overrelaxation (SPLOR) in conjunction with a piecewise continuous body fitted coordinate system is the first step is applying this method to the calculation of incompressible axisymmetric viscous/turbulent flow fields. The generally good agreement of present results with those of a second-order surface singularity method for the two potential flow cases presented gives some confidence in SPLOR.

An important feature of the algorithm is that line overrelaxation is maintained at junctions in the map where the mapping derivatives are discontinuous. This feature is a result of using backward differencing for q_ξ. Another important and well-known feature of the spline formulation is that the coefficient matrix associated with each line of unknowns is tridiagonal which leads to an efficient solution of the matrix equation.

Experience with the algorithm in its present form points to several shortcomings which can easily be corrected. These are:

1. Use of a constant step size in the ξ-direction does not allow for proper resolution in the vicinity of the rear stagnation point unless a very large number of intervals in ξ is used. This deficiency can be corrected by introduction of a stretching function in the ξ-direction to produce a nonuniform grid near the tail, or wherever else it is needed, so that the required accuracy can be achieved with a minimum number of intervals.
2. Application of the far-field boundary condition on a cylinder of finite radius is both cumbersome and restrictive. This feature can be removed by introducing an additional transformation in the η-direction to map an infinite radius into unity.

REFERENCES

1. D. F. Myring, "The Profile Drag of Bodies of Revolution in Subsonic Axisymmetric Flow," Royal Aircraft Establishment Technical Report 72234 (1972).

2. T. T. Huang, H. T. Want, N. Santelli, and N. C. Groves, "Propeller/Stern/Boundary-Layer Interaction on Axisymmetric Bodies: Theory and Experiment," David W. Taylor Naval Ship Research and Development Center Report 76-0113, December 1976.

3. G. H. Hoffman, "A Method for Calculating the Flow Field in the Tail Region of a Body of Revolution," Journal of Ship Research (to appear).

4. A Nakayama, V. C. Patel, and L. Landweber, "Flow Interaction Near the Tail of a Body of Revolution. Part 2: Iterative Solution for Flow Within and Exterior to Boundary Layer and Wake," Trans. ASME, Series I, J. Fluids Engin. 98, 538 (1976).

5. H. E. H. Mahgoub and P. Bradshaw, "Calculation of Turbulent - Inviscid Flow Interactions with Large Normal Pressure Gradients," AIAA Journal, 17, 1025 (1979).

6. J. A. Schetz and S. Favin, "Numerical Solution for the Near Wake of a Body with Propeller," Journal Hydronautics 11, 136 (1977).

7. J. A. Schetz and S. Favin, "Numerical Solution of a Body - Propeller Combination Flow Including Swirl and Comparisons with Data," Journal Hydronautics 13, 46 (1979).

8. J. D. Murphy, "An Efficient Numerical Method for the Solution of the Incompressible Navier-Stokes Equations," AIAA paper 77-171, AIAA 15th Aerospace Sciences Meeting, Los Angeles, CA, January 24-26, 1977.

9. G. K. Batchelor, "On Steady Laminar Flow with Closed Streamlines at Large Reynolds Numbers," J. Fluid Mech. 1, 177 (1956).

10. G. E. Chmielewski and G. H. Hoffman, "Finite-Difference Solution of an Elliptic Partial Differential Equation with Discontinuous Coefficients," International J. Numer. Meth. Engin. 12, 1407 (1978).

11. S. G. Rubin and P. K. Khosla, "Polynomial Interpolation for Viscous Flow Calculations," J. Comp. Phys. 24, 217 (1977).

12. H. B. Keller, "Accurate Difference Methods for Nonlinear Two-Point Boundary Value Problems," SIAM J. Numer. Anal. 11, 305 (1974).

13. J. Fernandez, "Flow Over an Axisymmetric Body in a Cylindrical Tunnel," TM 79-31, Applied Research Laboratory, The Pennsylvania State University, 1 March 1979.

14. V. C. Patel, A. Nakayama, and R. Damian, "Measurements in the Thick Axisymmetric Turbulent Boundary Layer Near the Tail of a Body of Revolution," J. Fluid Mech. 63, 345 (1974).

15. J. S. Parsons and R. E. Goodson, "The Optimum Shaping of Axisymmetric Bodies for Minimum Drag in Incompressible Flow," Purdue University Report ACC-72-6, June 1972.

16. V. C. Patel and Y. T. Lee, "Thick Axisymmetric Turbulent Boundary Layer and Near Wake of a Low-Drag Body of Revolution," Iowa Institute of Hydraulic Research, Iowa City, IA, Report No. 210, December 1977.

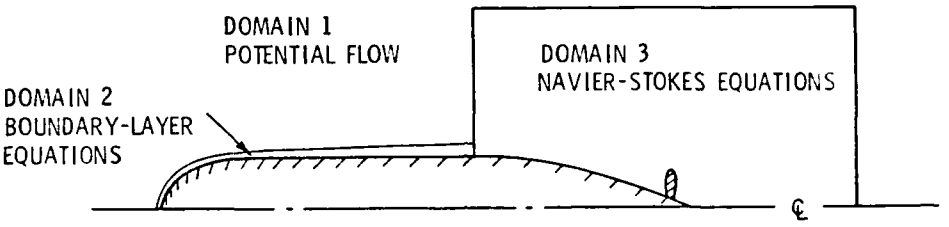

Figure 1. Flow Field Solution Domains.

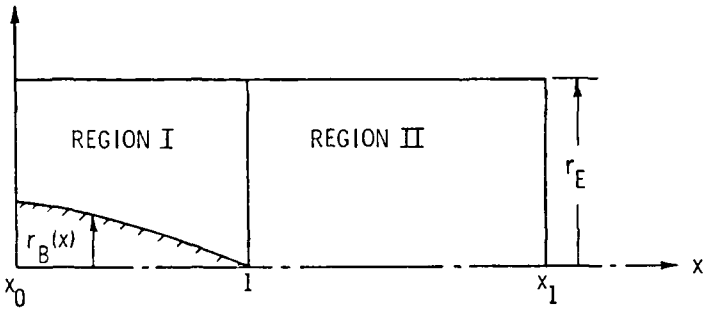

Figure 2. Truncated Computational Domain in the Tail-Near Wake Region of a Body of Revolution.

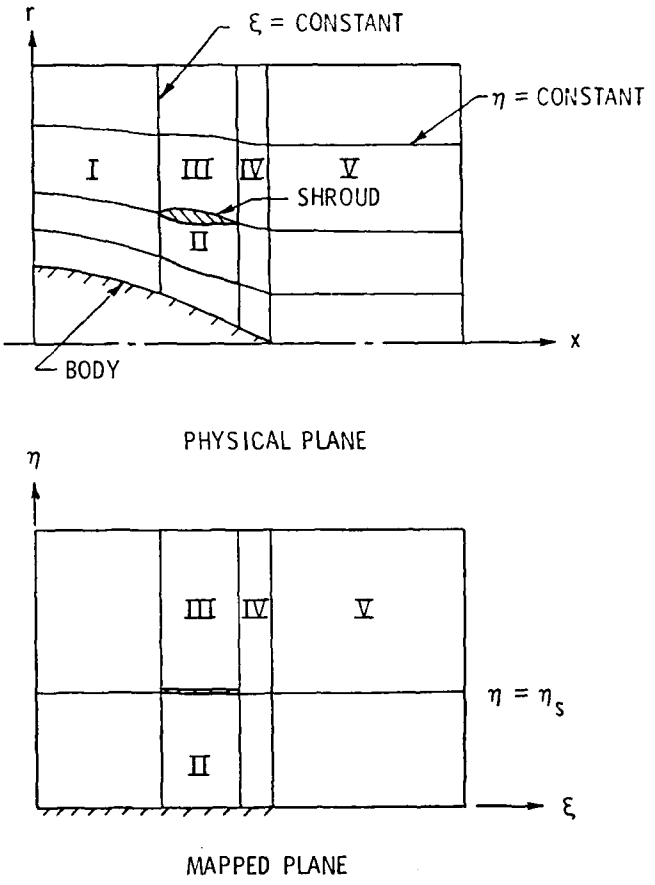

Figure 3. Typical Sheared Coordinate System for a Body - Shroud Combination.

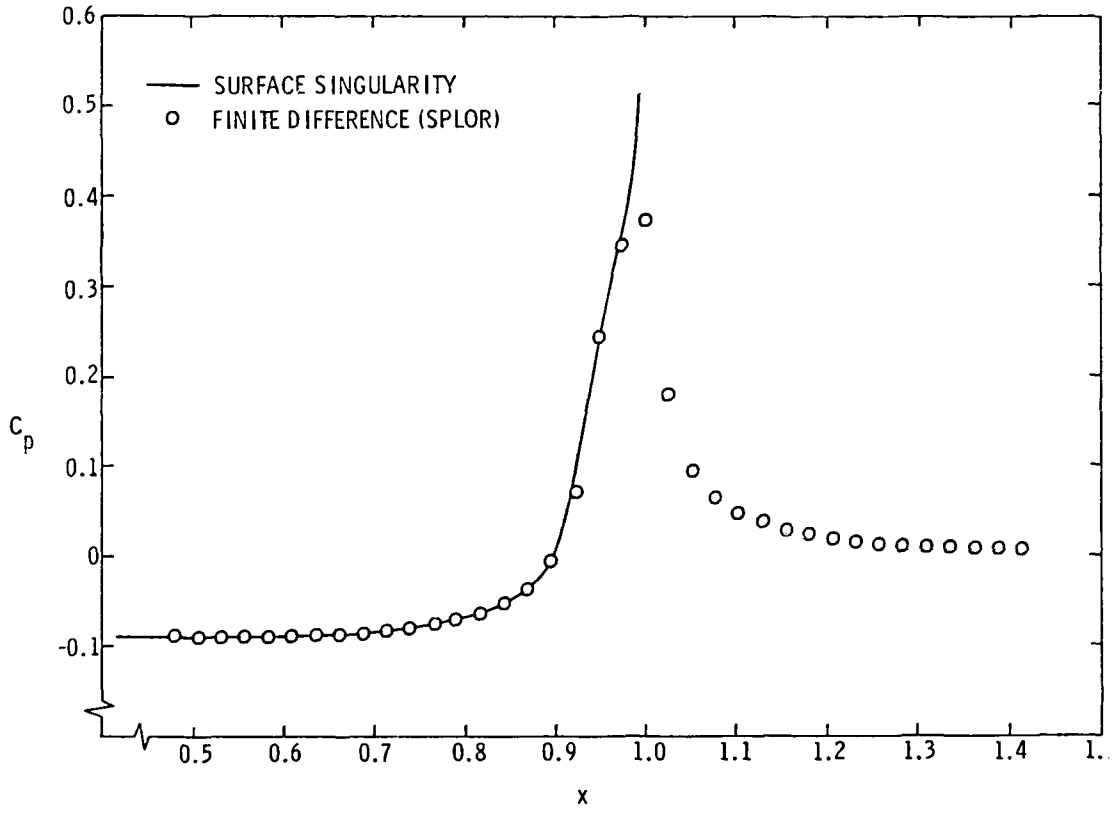

Figure 4. Body and Centerline Pressure Distribution for Modified Spheroid - Potential Flow.

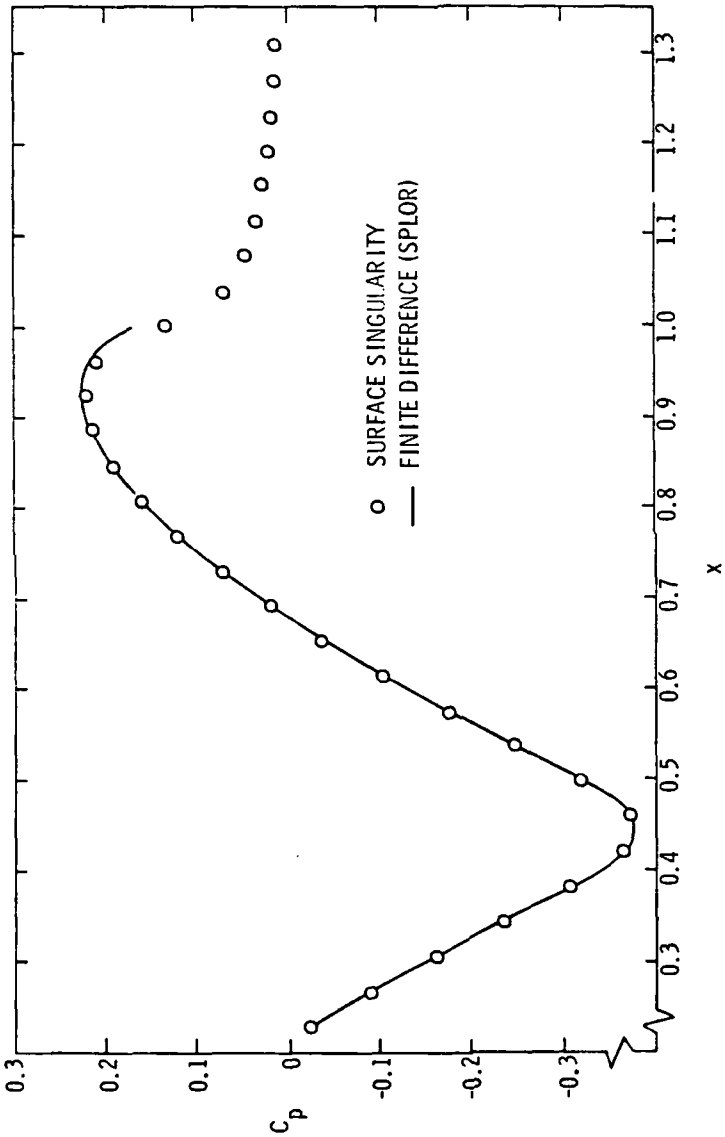

Figure 5. Body and Centerline Pressure Distribution for F-57 Body - Potential Flow.

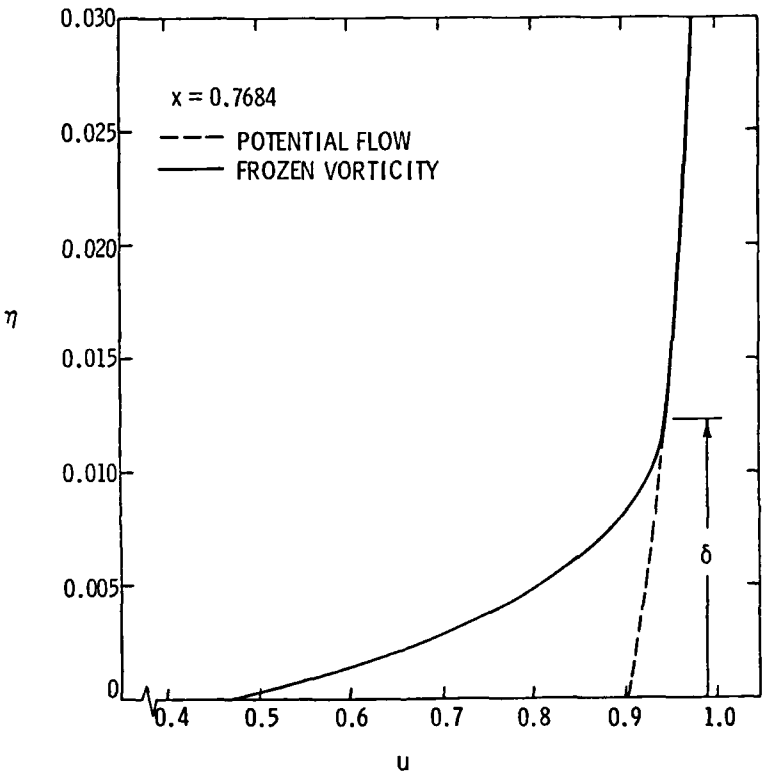

Figure 6. Initial Velocity Profile for Frozen Vorticity Test Case - F-57 Body.

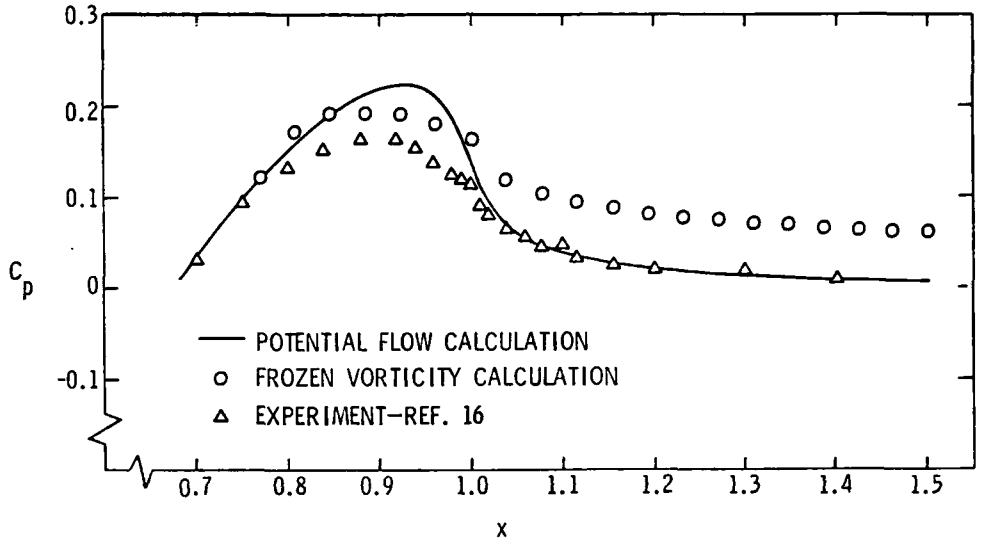

Figure 7. Frozen Vorticity and Potential Flow Body and Centerline Pressure Distribution for F-57 Body.

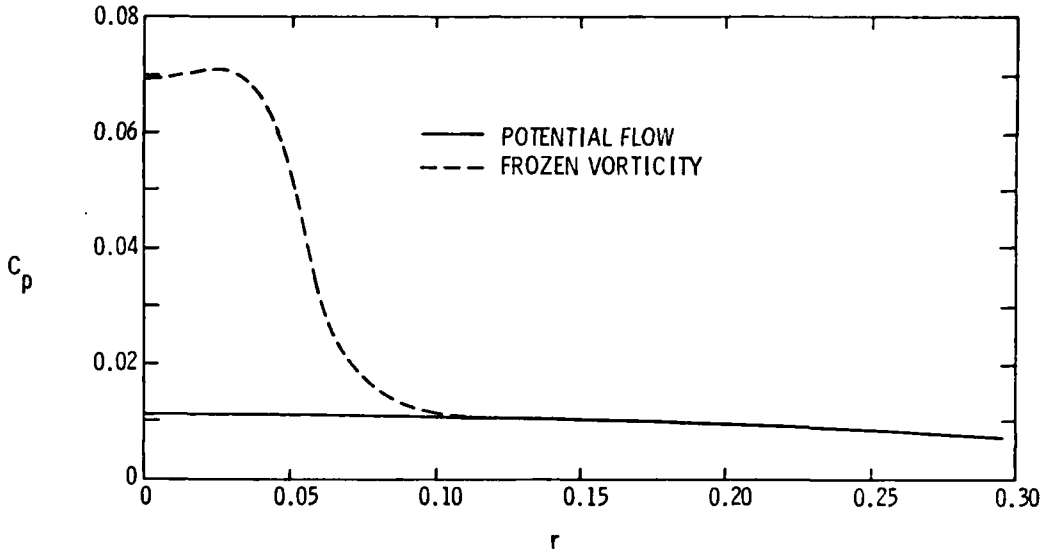

Figure 8. Pressure Profile Downstream of F-57 Body at x = 1.309.

DISTRIBUTION LIST FOR UNCLASSIFIED TM 80-108 by G. H. Hoffman, dated May 14, 1980

Commander
Naval Sea Systems Command
Department of the Navy
Washington, DC 20362
Attn: Library
Code NSEA-09G32
(Copy Nos. 1 and 2)

Naval Sea Systems Command
Attn: C. G. McGuigan
Code NSEA-63R2
(Copy No. 3)

Naval Sea Systems Command
Attn: E. G. Liszka
Code NSEA-63R1
(Copy No. 4)

Naval Sea Systems Command
Attn: G. Sorkin
Code NSEA-05R
(Copy No. 5)

Naval Sea Systems Command
Attn: T. E. Peirce
Code NSEA-63R-31
(Copy No. 6)

Naval Sea Systems Command
Attn: J. G. Juergens
Code NSEA-05H
(Copy No. 7)

Naval Sea Systems Command
Attn: H. C. Claybourne
Code NSEA-05H5
(Copy No. 8)

Naval Sea Systems Command
Attn: A. R. Paladino
Code NSEA-05H1
(Copy No. 9)

Naval Sea Systems Command
Attn: F. J. Welling
Code NSEA-521
(Copy No. 10)

Commanding Officer
Naval Underwater Systems Center
Newport, RI 02840
Attn: C. N. Pryor
Code 01
(Copy No. 11)

Naval Underwater Systems Center
Attn: D. Goodrich
Code 36301
(Copy No. 12)

Naval Underwater Systems Center
Attn: R. H. Nadolink
Code 3634
(Copy No. 13)

Naval Underwater Systems Center
Attn: R. Trainor
Code 36314
(Copy No. 14)

Naval Underwater Systems Center
Attn: F. White
Code 36314
(Copy No. 15)

Naval Underwater Systems Center
Attn: Library
Code 54
(Copy No. 16)

Commanding Officer
Naval Ocean Systems Center
San Diego, CA 92152
Attn: D. Nelson
Code 6342
(Copy No. 17)

Commanding Officer and Director
David W. Taylor Naval Ship R&D Center
Department of the Navy
Bethesda, MD 20084
Attn: W. B. Morgan
Code 154
(Copy No. 18)

David W. Taylor Naval Ship R&D Center
Attn: R. Cumming
Code 1544
(Copy No. 19)

David W. Taylor Naval Ship R&D Center
Attn: T. T. Huang
Code 1552
(Copy No. 20)

David W. Taylor Naval Ship R&D Center
Attn: J. McCarthy
Code 1552
(Copy No. 21)

DISTRIBUTION LIST FOR UNCLASSIFIED TM 80-108 by G. H. Hoffman, dated May 14, 1980

David W. Taylor Naval Ship R&D Center
Attn: M. Sevik
Code 19
(Copy No. 22)

David W. Taylor Naval Ship R&D Center
Attn: Library
Code 522
(Copy No. 23)

Commanding Officer and Director
David W. Taylor Naval Ship R&D Center
Department of the Navy
Annapolis Laboratory
Annapolis, MD 21402
Attn: J. G. Stricker
Code 2721
(Copy No. 24)

Commander
Naval Surface Weapons Center
Silver Spring, MD 20910
Attn: G. C. Gaunaurd
Code R-31
(Copy No. 25)

Naval Surface Weapons Center
Attn: J. L. Baldwin
Code WA-42
(Copy No. 26)

Naval Surface Weapons Center
Attn: W. J. Glowacki
Code R-44
(Copy No. 27)

Naval Surface Weapons Center
Attn: J. M. Solomon
(Copy No. 28)

Office of Naval Research
Department of the Navy
800 N. Quincy Street
Arlington, VA 22217
Attn: R. Cooper
Code 438
(Copy No. 29)

Office of Naval Research
Attn: H. Fitzpatrick
Code 438
(Copy No. 30)

Defense Technical Information Center
5010 Duke Street
Cameron Station
Alexandria, VA 22314
(Copy Nos. 31 to 42)

National Bureau of Standards
Aerodynamics Section
Washington, DC 20234
Attn: P. S. Klebanoff
(Copy No. 43)

Rand Corporation
1700 Main Street
Santa Monica, CA 90406
Attn: C. Gazley
(Copy No. 44)

California Institute of Technology
Jet Propulsion Laboratory
4800 Oak Grove Drive
Pasadena, CA 91103
Attn: Dr. Leslie Mack
(Copy No. 45)

Iowa Institute of Hydraulic Research
The University of Iowa
Iowa City, Iowa 52240
Attn: V. C. Patel
(Copy No. 46)

Dynamics Technology, Inc.
3838 Carson Street, Suite 110
Torrance, CA 90503
Attn: Wayne H. Haigh
(Copy No. 47)

The Pennsylvania State University
Applied Research Laboratory
Post Office Box 30
State College, PA 16801
Attn: J. J. Eisenhuth
(Copy No. 48)

Applied Research Laboratory
Attn: R. E. Henderson
(Copy No. 49)

Applied Research Laboratory
Attn: G. H. Hoffman
(Copy No. 50)

DISTRIBUTION LIST FOR UNCLASSIFIED TM 80-108 by G. H. Hoffman, dated May 14, 1980

Applied Research Laboratory
Attn: B. E. Robbins
(Copy No. 51)

Applied Research Laboratory
Attn: Garfield Thomas Water Tunnel Files
(Copy No. 52)

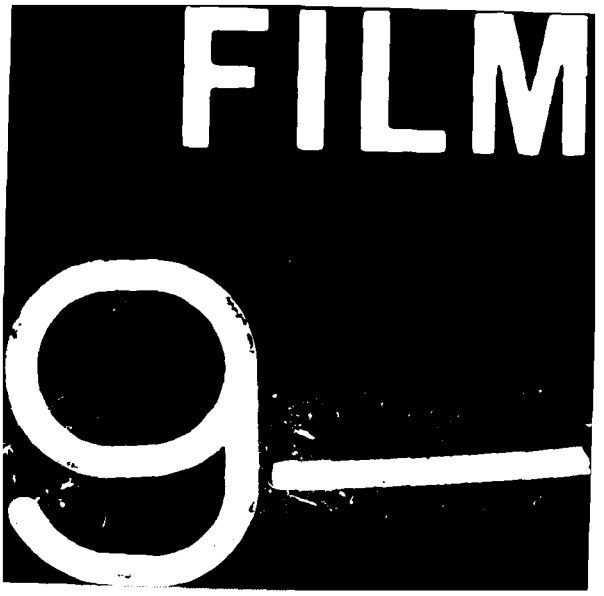
FILM
9